Research Square

Preprints are preliminary reports that have not undergone peer review.
They should not be considered conclusive, used to inform clinical practice,
or referenced by the media as validated information.

Network Pharmacology, Molecular Docking, and In Vitro Validation Suggest that Xiaoluo Wan Attenuates Central Precocious Puberty via the Bile Acid–TGR5–PI3K/Akt Axis

Jiayi Kang[1]
Foshan Clinical Medical College, Guangzhou University of Chinese Medicine
Zilun Wu[2]
Foshan Clinical Medical College, Guangzhou University of Chinese Medicine
Hongjie Liu[1]
Foshan Clinical Medical College, Guangzhou University of Chinese Medicine
Shan Mo
1549505114@qq.com
Foshan Fosun Chancheng Hospital
Jun Lu
Foshan Fosun Chancheng Hospital
Jianlei Liu
Foshan Fosun Chancheng Hospital
Chunmei He
Foshan Fosun Chancheng Hospital
Shengzhen Wu
Foshan Fosun Chancheng Hospital
Shanshan He
Foshan Fosun Chancheng Hospital

Article

Keywords: Xiaoluo Wan, central precocious puberty, network pharmacology, molecular docking, bile acids, TGR5, PI3K/Akt, GT1-7 cells, traditional Chinese medicine

Posted Date: November 26th, 2026

DOI: https://doi.org/10.21203/rs.3.rs-11253346/v1

License: This work is licensed under a Creative Commons Attribution 4.0 International License.
Read Full License

Additional Declarations: No competing interests reported.

Network Pharmacology, Molecular Docking, and In Vitro Validation Suggest that Xiaoluo Wan Attenuates Central Precocious Puberty via the Bile Acid–TGR5–PI3K/Akt Axis

Jiayi Kang[1]†, Zilun Wu[1]†, Hongjie Liu[1], Jianlei Liu[2], Chunmei He[2], Shengzhen Wu[2], Shanshan He[2], Jun Lu[2]*, Shan Mo[2]*

[1] Foshan Clinical Medical College, Guangzhou University of Chinese Medicine, Foshan, Guangdong, China

[2] Foshan Fosun Chancheng Hospital, Foshan, Guangdong, China

*Corresponding authors: Shan Mo, Professor. Foshan Fosun Chancheng Hospital, Foshan, Guangdong, China. E-mail: 1549505114@qq.com; Jun Lu, Foshan Fosun Chancheng Hospital, Foshan, Guangdong, China. E-mail: lujun@fsccyy.com

†These authors contributed equally: Jiayi Kang and Zilun Wu.

Abstract

Background: Central precocious puberty (CPP), defined as the premature reactivation of the hypothalamic–pituitary–gonadal axis, is increasingly prevalent in children, particularly in the context of childhood obesity. Emerging evidence implicates bile acid signalling—especially the muricholic acid (MCA)–TGR5–PI3K/Akt pathway—as a metabolic link between obesity and early pubertal onset. Xiaoluo Wan (XLW), a classical traditional Chinese medicine (TCM) formula composed of Scrophulariae Radix (Xuanshen), Fritillariae Thunbergii Bulbus (Zhebeimu), and Ostreae Concha (Muli), has long been used clinically for TCM syndromes associated with precocious puberty; however, its underlying pharmacological mechanisms remain unclear. This study aimed to systematically predict the bioactive compounds, potential targets, and signalling pathways of XLW against CPP using network pharmacology and molecular docking, and to validate the core predictions in a GnRH neuronal cell model.

Methods: Candidate compounds of XLW were retrieved from the TCMSP and BATMAN-TCM databases and screened by oral bioavailability, drug-likeness, molecular weight, and SwissADME pharmacokinetic criteria. Compound-related targets were predicted with SwissTargetPrediction. CPP-related genes were collected from GeneCards, OMIM, DrugBank, and DisGeNET. Intersection targets were subjected to protein–protein interaction (PPI) network analysis (STRING) with multi-round topological screening (CytoNCA) in Cytoscape, GO and KEGG enrichment analysis (DAVID), and construction of a "herb–compound–target–disease" network. Molecular docking between representative compounds and core targets was performed using AutoDock Vina. For in vitro validation, mouse hypothalamic GT1-7 GnRH neuronal cells were stimulated with MCA (100 nM) in the presence or absence of XLW; GnRH secretion was measured by ELISA, and TGR5–PI3K/Akt pathway proteins were examined by Western blotting, with the TGR5 antagonist SBI-115 used for mechanistic interrogation.

Results: Sixteen candidate active compounds and 555 compound-related targets were obtained, among which 260 overlapped with 3,046 CPP-related genes. Topological screening of the PPI network identified 15 core targets, including SRC, ESR1, AKT1,

STAT3, and EGFR. GO analysis yielded 3,283 enriched terms, and KEGG analysis yielded 190 pathways, prominently featuring the GnRH secretion and signalling pathways, oestrogen signalling, steroid hormone biosynthesis, neuroactive ligand–receptor interaction, insulin signalling, and adipocytokine signalling. Beta-sitosterol, sugiol, sitosterol, and harpagoside emerged as the most highly connected compounds, and molecular docking showed strong predicted affinities with core targets (e.g., beta-sitosterol–AKT1, −10.980 kcal/mol; sugiol–AKT1, −9.975 kcal/mol). In GT1-7 cells, XLW showed no cytotoxicity up to 10,000 μg/mL. MCA markedly increased GnRH secretion (from 6.143 ± 0.201 to 21.470 ± 1.219 pg/mL, $p < 0.0001$), whereas co-treatment with XLW (250 μg/mL) almost completely abolished this effect (5.179 ± 0.312 pg/mL, $p < 0.0001$ vs. MCA). Western blot analyses showed that XLW attenuated MCA-induced upregulation of TGR5, PI3K, and Akt phosphorylation, and that this modulation was diminished by the TGR5 antagonist SBI-115.

Conclusions: XLW may attenuate CPP through a multi-compound, multi-target, and multi-pathway network centred on AKT1/SRC/ESR1/STAT3/EGFR and converging on the PI3K/Akt, GnRH, and oestrogen signalling pathways. Preliminary in vitro evidence supports that XLW suppresses MCA-induced GnRH hypersecretion at least partly through the TGR5–PI3K/Akt axis, providing a pharmacological rationale and prioritised hypotheses for further mechanistic and in vivo studies.

Keywords: Xiaoluo Wan; central precocious puberty; network pharmacology; molecular docking; bile acids; TGR5; PI3K/Akt; GT1-7 cells; traditional Chinese medicine

1. Introduction

Central precocious puberty (CPP) is a paediatric endocrine disorder characterised by the premature reactivation of the hypothalamic–pituitary–gonadal axis (HPGA), defined clinically by the development of secondary sexual characteristics before the age of 7.5 years in girls and 9 years in boys [1,2]. The incidence of CPP has risen markedly worldwide in recent decades, and early pubertal development is associated with premature epiphyseal closure and compromised adult height, as well as increased long-term risks of obesity, metabolic syndrome, polycystic ovary syndrome, and hormone-dependent malignancies [3].

Epidemiological studies consistently indicate that obesity is a major risk factor for early pubertal onset, with obese children exhibiting a two- to three-fold higher risk of precocious puberty than their normal-weight peers [4,5]. Excess adiposity is thought to accelerate pubertal timing through metabolic signals—including leptin, insulin, and inflammatory cytokines—that converge on hypothalamic kisspeptin–KISS1R signalling and gonadotropin-releasing hormone (GnRH) neurons [6–8]. However, the molecular mechanisms by which metabolic derangements are translated into premature HPGA activation remain incompletely understood.

Recent advances in bile acid biology have provided a compelling new framework. Beyond their classical role in lipid digestion, bile acids are now recognised as endocrine signalling molecules acting through the membrane receptor TGR5 (GPBAR1) and the nuclear receptor FXR to regulate energy metabolism, inflammation, and neuroendocrine function [9–12]. In 2024, Vanden Brink and colleagues demonstrated that the circulating bile acid pool shifts across pubertal maturation in girls and rats, that hypothalamic Tgr5 expression increases during the pubertal transition, that TGR5 activation stimulates GnRH release from hypothalamic explants in a kisspeptin-receptor-dependent manner, and that early overexpression of TGR5 in the arcuate nucleus advances pubertal onset in female rats [13]. More recently, Wang et al. reported in PNAS that muricholic acid (MCA) species are elevated in the serum of girls with CPP, that MCA accumulates in the hypothalamus under high-fat-diet conditions and activates TGR5 on GnRH neurons, thereby enhancing GnRH expression via the TGR5–PI3K/Akt–mTOR signalling cascade;

conversely, lowering MCA levels delayed high-fat-diet-induced precocious puberty, whereas TGR5 knockout protected female mice from it [14]. These findings establish the MCA–TGR5–PI3K/Akt axis as a critical molecular link between metabolic status and the timing of pubertal initiation, and nominate it as a promising therapeutic target.

The PI3K/Akt pathway occupies a central position in this cascade. As a pivotal intracellular signalling hub governing cell growth, metabolism, survival, and neuroendocrine function, aberrant PI3K/Akt activation in hypothalamic neurons can directly modulate GnRH synthesis and secretion [15,16]. Notably, previous network pharmacology studies of classical TCM formulas used for CPP, such as Dabuyin Wan and Zhibai Dihuang Wan, have repeatedly identified the PI3K/Akt pathway as the most significantly enriched pathway, pointing to it as a shared molecular target of TCM interventions in precocious puberty.

Xiaoluo Wan (XLW), first recorded in the Qing-dynasty medical classic "Yi Xue Xin Wu" (Medical Insights) by Zhong-ling Cheng, is composed of three herbs in equal proportions: Scrophulariae Radix (Xuanshen), Fritillariae Thunbergii Bulbus (Zhebeimu), and Ostreae Concha (Muli) [17]. In TCM theory, the formula nourishes yin, clears heat, resolves phlegm, and dissipates nodules; building on the core pathogenesis of "yin deficiency with effulgent fire and phlegm coagulation" in paediatric precocious puberty, modern practitioners have extended its application to CPP, with particularly favourable effects in girls with premature thelarche and firm breast nodules [18]. Modern pharmacological studies indicate that Scrophulariae Radix contains iridoid glycosides (harpagide, harpagoside) with anti-inflammatory and metabolic regulatory activities [19], that Fritillariae Thunbergii Bulbus contains steroidal alkaloids (peimine, peiminine) capable of modulating lipid metabolism and PI3K/Akt/mTOR signalling [20,21], and that Ostreae Concha provides bioactive peptides, taurine, and trace elements (zinc, selenium) relevant to hypothalamic neuroendocrine regulation and gonadal development [18]. Nevertheless, the systematic pharmacological basis and the "compound–target–pathway" mechanism by which XLW acts against CPP—especially in relation to the newly recognised bile acid–TGR5–PI3K/Akt axis—have not been elucidated.

Network pharmacology, an approach that integrates systems biology, bioinformatics, and pharmacology, is particularly suited to dissecting the multi-component, multi-target nature of TCM formulas [22]. Combined with molecular docking, it provides an efficient strategy for predicting bioactive compounds, core targets, and signalling pathways before experimental validation. In the present study, we applied an integrated network pharmacology and molecular docking strategy to (i) identify the candidate active compounds of XLW and their targets, (ii) delineate the core targets and pathways shared with CPP, and (iii) evaluate the binding capacity of representative compounds to core targets. Furthermore, we experimentally validated the core prediction—that XLW restrains GnRH hypersecretion through TGR5–PI3K/Akt signalling—in MCA-stimulated GT1-7 hypothalamic GnRH neuronal cells. Our aim was to provide a testable pharmacological rationale for the clinical use of XLW in CPP and a prioritised list of hypotheses for subsequent in-depth mechanistic and in vivo studies.

2. Materials and Methods

2.1. Screening of Candidate Active Compounds and Targets of Xiaoluo Wan

Chemical constituents of the component herbs of XLW were retrieved from the Traditional Chinese Medicine Systems Pharmacology Database and Analysis Platform (TCMSP, https://www.tcmspe.com/) and the Bioinformatics Analysis Tool for Molecular mechANism of Traditional Chinese Medicine (BATMAN-TCM, http://bionet.ncpsb.org.cn/batman-tcm/) [23,24]. For Scrophulariae Radix and Fritillariae Thunbergii Bulbus, compounds recorded in TCMSP were filtered using oral bioavailability (OB) ≥ 30%, drug-likeness (DL) ≥ 0.18, and molecular weight (MW) ≤ 500. The retained compounds were further evaluated with the SwissADME platform (http://www.swissadme.ch/), and only compounds with high predicted gastrointestinal (GI) absorption and at least three favourable drug-likeness criteria were retained [25]. Because Ostreae Concha (an animal/mineral-derived medicinal) is not covered by TCMSP, its constituents and targets were retrieved from BATMAN-TCM using "Herb"

as the input type, with a score cut-off of 20 and $P < 0.05$. Potential targets of the final set of compounds were predicted using SwissTargetPrediction (http://www.swisstargetprediction.ch/) [26]. Protein annotations and gene symbols were standardised using the UniProt database (https://www.uniprot.org/) [27], and duplicated compounds, duplicated targets, and synonymous genes were merged to generate the compound–target dataset for subsequent network analysis.

2.2. Collection of CPP-Related Disease Targets

Using "central precocious puberty" as the query term, disease-related genes were retrieved from GeneCards (https://www.genecards.org/), the Online Mendelian Inheritance in Man database (OMIM, https://www.omim.org/), DrugBank (https://www.drugbank.ca/), and DisGeNET (https://www.disgenet.org/) [28–31]. Genes obtained from the different databases were merged, de-duplicated, and standardised to official human gene symbols. The intersection between compound-related targets and disease-related genes was computed with the Venny 2.1 platform, yielding the candidate therapeutic targets of XLW against CPP.

2.3. Construction of the "Herb–Compound–Target–Disease" Network

Correspondence tables of "herb–compound", "compound–target", and "target–disease" relationships were established and imported into Cytoscape 3.10 (https://cytoscape.org/) to construct the "herb–compound–target–CPP" regulatory network [32]. Herbs, compounds, and target genes were represented by nodes with distinct shapes and colours, and edges represented their associations. The NetworkAnalyzer plugin was used to compute topological parameters of each node, including degree, betweenness centrality, closeness centrality, eigenvector centrality, local average connectivity (LAC), and network centrality, and key compounds and candidate core targets were screened according to these topological features.

2.4. Protein–Protein Interaction Network Analysis and Core Target Screening

The candidate therapeutic targets were submitted to the STRING database (https://string-db.org/) for PPI analysis, with the species restricted to Homo sapiens and the combined score threshold set to ≥ 0.95 [33]. After removal of disconnected protein nodes, the network was imported into Cytoscape 3.10, and the CytoNCA plugin was used to compute node topology metrics (degree, betweenness, closeness, eigenvector, LAC, and network centrality) [34]. A multi-round (three-level) topological screening procedure was applied to progressively narrow down the network and identify core targets.

2.5. GO and KEGG Enrichment Analysis

The intersection targets were subjected to Gene Ontology (GO) functional annotation and Kyoto Encyclopedia of Genes and Genomes (KEGG) pathway enrichment analysis using the DAVID database (https://david.ncifcrf.gov/) [35–39]. GO analysis covered three categories: biological process (BP), cellular component (CC), and molecular function (MF). Enrichment results were ranked by P value and visualised jointly with the gene ratio and the number of enriched genes. Bubble plots, bar charts, and pathway maps were generated with R software (version 4.5.2). In addition, enrichment terms were screened against the known pathophysiology of CPP to identify entries related to the HPGA and central neuroendocrine regulation.

2.6. Molecular Docking

Representative active compounds and core targets identified by network pharmacology were selected for molecular docking. Three-dimensional structures of small-molecule ligands were obtained from the PubChem database (https://pubchem.ncbi.nlm.nih.gov/) [40], and crystal structures of receptor proteins were retrieved from the RCSB Protein Data Bank (https://www.rcsb.org/) [41]. Receptor structures were pre-processed by chain selection, removal of non-target heteroatoms, hydrogenation, and charge calculation, and the active pocket and grid-box parameters were defined according to the position of the co-crystallised ligand; ligands and receptors

were converted to PDBQT format. Ligand–receptor docking was performed with AutoDock Vina 1.2.7, and binding affinity (kcal/mol) was used to evaluate the predicted binding capacity of each combination [42,43]. Representative complex conformations were selected, and three-dimensional diagrams of the overall protein–ligand structures and binding pockets were rendered with PyMOL 3.1.8 (Schrödinger, LLC) [44].

2.7. Preparation of Xiaoluo Wan Water Extract

The crude drugs of Xiaoluo Wan were commercially purchased, and all complied with the standards of the Pharmacopoeia of the People's Republic of China (2020 edition) [18]: Scrophulariae Radix (Xuanshen; origin: Jinhua, Zhejiang Province, China; supplier: Guangdong Yuanshengtai Pharmaceutical Co., Ltd.; batch No. 26070104), Fritillariae Thunbergii Bulbus (Zhebeimu; origin: Zhejiang Province, China; supplier: Sinopharm Group Fengliaoxing (Foshan) Medicinal Materials and Decoction Pieces Co., Ltd.; batch No. C22603155), and Ostreae Concha (Muli; origin: Yangjiang, Guangdong Province, China; supplier: Guangdong Yuanshengtai Pharmaceutical Co., Ltd.; batch No. 26060105). All three crude drugs were cultivated medicinal materials obtained through commercial channels and were not collected from the wild; therefore, no field-collection permits were required. The crude drugs were authenticated by Shengzhen Wu (Foshan Fosun Chancheng Hospital, Foshan, China) according to the standards of the Pharmacopoeia of the People's Republic of China (2020 edition) [18], and voucher specimens corresponding to the supplier batch numbers listed above are deposited at the Precision Oncology Key Laboratory of Foshan Fosun Chancheng Hospital. The three drugs were mixed at a 1:1:1 ratio. Ostreae Concha was pre-decocted; the mixed crude drugs were then soaked in ten volumes of purified water for 30 min and decocted at a gentle boil for 1.5 h. The decoction was filtered through four layers of sterile gauze, and the residue was decocted again with eight volumes of water for 1 h. The two filtrates were combined, concentrated under reduced pressure at 45 °C to a concentration equivalent to 1 g of crude drug per mL, sterilised by vacuum filtration through a 0.22-μm membrane, aliquoted, and stored frozen until use.

2.8. Cell Culture

Immortalised mouse hypothalamic GnRH neuronal GT1-7 cells (purchased from iCell Bioscience Co., Ltd., Shanghai, China), a well-established model for studying the regulation of GnRH secretion [45], were cultured in high-glucose Dulbecco's modified Eagle medium (DMEM) supplemented with 10% fetal bovine serum and 1% penicillin–streptomycin at 37 °C in a humidified atmosphere of 5% CO_2. Cell identity was authenticated by multiplex QPCR-based species identification, which confirmed mouse origin with no detectable human, rat, or hamster cell contamination. Cells in the logarithmic growth phase with good morphology were used for experiments.

2.9. Cell Viability Assay (Alamar Blue)

GT1-7 cells were seeded into 96-well plates at 3×10^3 cells per well. After 24 h of adherence, the cells were treated with XLW water extract at final concentrations of 0, 500, 1,000, 5,000, 10,000, 12,500, and 15,000 μg/mL for 24 h. Cell viability was then measured with the Alamar Blue assay according to the manufacturer's instructions, and absorbance was read with a microplate reader. A cell viability of ≥ 80% relative to the untreated control was defined as the safety threshold for subsequent experiments.

2.10. MCA-Induced GnRH Hypersecretion Model and Drug Intervention

To mimic the aberrant bile acid signalling observed in obesity-related CPP, GT1-7 cells were stimulated with muricholic acid (MCA, 100 nM) as previously described [14]. In dose-finding experiments, cells were divided into a blank control group, an MCA model group, and MCA + XLW groups at 100, 250, and 500 μg/mL. For mechanistic experiments, four groups were used: blank control, MCA model, XLW alone (250 μg/mL), and MCA + XLW (250 μg/mL). In TGR5 intervention experiments, the TGR5-specific antagonist SBI-115 (10 μM) was applied alone or in combination with MCA and XLW, yielding five groups: normal control, MCA model, MCA + SBI-115, MCA + XLW (250 μg/mL), and MCA + XLW + SBI-115. After 24 h of treatment, cell culture supernatants and cell pellets were collected for ELISA and Western blot analyses.

2.11. GnRH Secretion Assay (ELISA)

GnRH concentrations in cell culture supernatants were measured using a mouse GnRH enzyme-linked immunosorbent assay (ELISA) kit according to the manufacturer's instructions. A standard curve was constructed for each assay, and sample concentrations were calculated accordingly.

2.12. Western Blotting

Total protein was extracted from GT1-7 cells with RIPA lysis buffer, and protein concentrations were determined with a BCA assay. Equal amounts of protein were separated by SDS-PAGE and transferred to PVDF membranes by wet transfer. After blocking with 5% skimmed milk, membranes were incubated overnight at 4 °C with primary antibodies against TGR5, PI3K, phospho-Akt (Ser473), Akt, GPER, and GAPDH (all 1:1,000), followed by horseradish peroxidase-conjugated secondary antibodies (1:5,000) for 1 h at room temperature. Bands were visualised by enhanced chemiluminescence, and band intensities were quantified by densitometry and normalised to GAPDH; Akt activation was evaluated as the ratio of phosphorylated to total Akt.

2.13. Statistical Analysis

Data are expressed as mean ± standard deviation (SD) from at least three independent experiments. Differences among groups were analysed by one-way analysis of variance (ANOVA) followed by Dunnett's or Tukey's multiple comparisons test, as appropriate, using GraphPad Prism software. A two-sided P value < 0.05 was considered statistically significant.

3. Results

3.1. Candidate Active Compounds and Potential Targets of XLW Against CPP

Screening of the TCMSP database with "Fritillariae Thunbergii Bulbus" and "Scrophulariae Radix" as keywords yielded 7 and 6 records of active compounds, respectively. Searching BATMAN-TCM for Ostreae Concha retrieved 6 active compounds and 33 compound–target associations. After merging, 19 candidate compound records were obtained; after removal of duplicated compounds and compounds without valid corresponding targets, 16 compound nodes entered the regulatory network (Mol IDs re-assigned). Target prediction with SwissTargetPrediction yielded 1,329 compound–target records, corresponding to 555 unique gene symbols after merging and de-duplication. Disease-target retrieval returned 2,979 genes from GeneCards, 3 from DrugBank, 88 from DisGeNET, and 99 from OMIM, for a total of 3,046 CPP-related genes after integration and de-duplication. Intersection of compound targets with disease genes identified 260 potential therapeutic targets of XLW against CPP (Fig. 1).

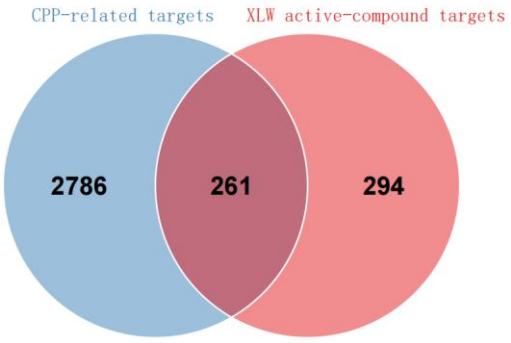

Fig. 1. Venn diagram of the intersection between Xiaoluo Wan compound targets and CPP-related disease genes.

3.2. PPI Network Analysis and Core Target Screening

The 260 potential therapeutic targets were imported into STRING (species: Homo sapiens), yielding 750 interaction records. After removal of disconnected nodes, a multi-round CytoNCA topological screening was performed: the first, second, and third rounds retained 182, 45, and 15 nodes, respectively (Figs. 2 and 3). The final core target set comprised AR, HSP90AA1, HSP90AB1, AKT1, ERBB2, EP300, STAT3, EGFR, ESR1, JUN, SRC, MAPK1, MAPK3, PIK3CA, and PTPN11, among which SRC, ESR1, AKT1, STAT3, and EGFR exhibited the highest network centrality (Table 1).

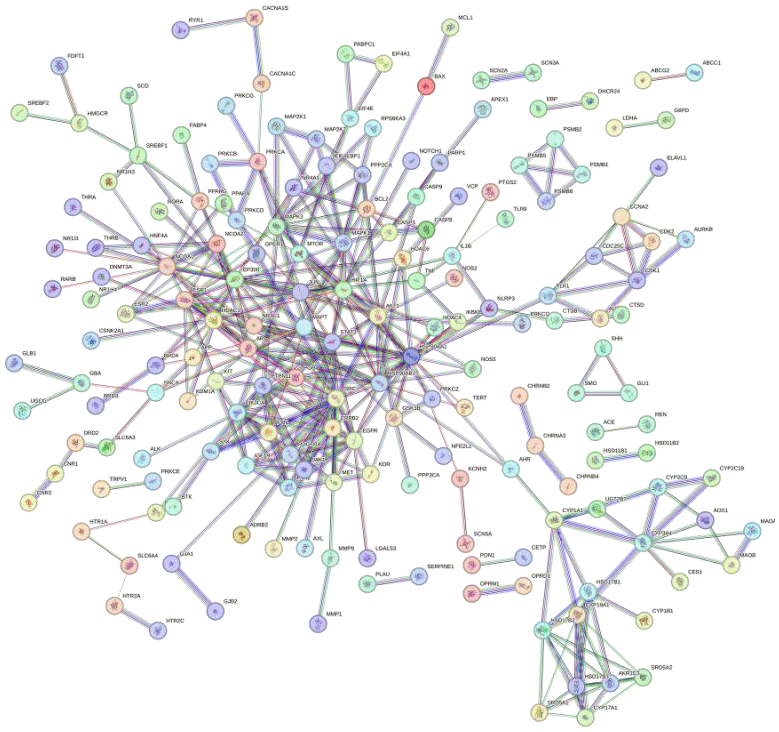

Fig. 2. Protein–protein interaction network of the potential targets of Xiaoluo Wan against CPP (STRING).

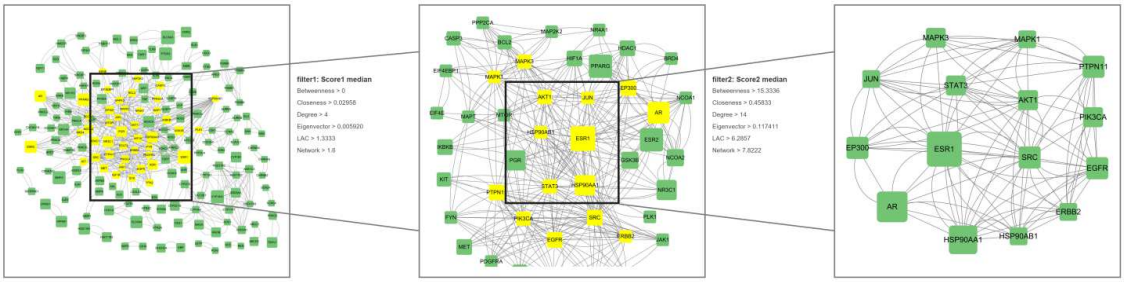

Fig. 3. Three-level core PPI network obtained by multi-round CytoNCA topological screening.

Table 1. Core targets of Xiaoluo Wan against CPP identified by three-level topological screening.

Rank tier	**Core targets (gene symbols)**
Highest-centrality nodes	SRC, ESR1, AKT1, STAT3, EGFR
Remaining core nodes	AR, HSP90AA1, HSP90AB1, ERBB2, EP300, JUN, MAPK1, MAPK3, PIK3CA, PTPN11

3.3. GO Functional and KEGG Pathway Enrichment Analysis

GO enrichment analysis of the 260 potential targets returned 3,283 records. Enriched biological processes mainly involved the sterol metabolic process, response to steroid hormones, response to peptide hormones, response to oxygen levels and hypoxia, response to xenobiotic stimuli, intracellular receptor signalling pathways, and regulation of membrane potential. Enriched cellular components mainly involved the cell membrane, cytoplasm, nucleus, cytosol, extracellular region, and extracellular space. Enriched molecular functions mainly involved protein binding, ATP binding, metal-ion binding, protein kinase activity, enzyme binding, and DNA binding.

KEGG enrichment analysis returned 190 records. Top-ranked pathways included chemical carcinogenesis–receptor activation, EGFR tyrosine kinase inhibitor resistance, the HIF-1 signalling pathway, thyroid hormone signalling, proteoglycans in cancer, lipid and atherosclerosis, endocrine resistance, and oestrogen signalling (Fig. 4).

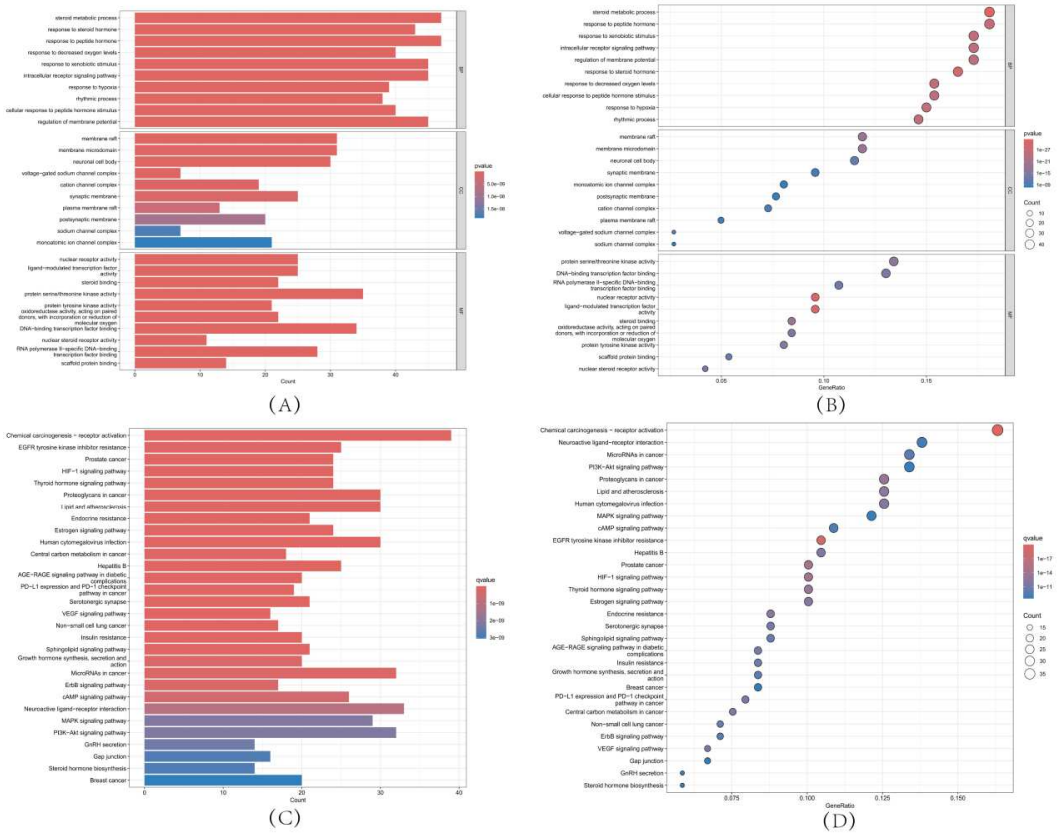

Fig. 4. GO and KEGG enrichment analysis of the potential targets of Xiaoluo Wan against CPP. KEGG pathway annotations were obtained from the KEGG database [36–38] (www.kegg.jp/kegg/kegg1.html).

When the enrichment results were further screened against the pathophysiology of CPP, a subset of terms closely related to the HPGA and central neuroendocrine regulation emerged (Fig. 5). Relevant GO entries included the regulation of gonadotropin secretion, response to gonadotropins, reproductive system development, primary sexual characteristic development, steroid hormone metabolism and biosynthesis, oestrogen receptor signalling, and androgen metabolism, as well as neurotransmitter-related processes such as dopamine metabolism and transport and GABAergic and glutamatergic synaptic transmission. CPP-relevant KEGG pathways included GnRH secretion, the GnRH signalling pathway, oestrogen signalling, steroid hormone biosynthesis, ovarian steroidogenesis, neuroactive ligand–receptor interaction, dopaminergic synapse, GABAergic synapse, glutamatergic synapse, and calcium signalling. In addition, insulin resistance, insulin signalling, adipocytokine signalling, circadian regulation, thyroid

hormone signalling, and growth hormone synthesis, secretion, and action were also significantly enriched. These results link the targets of XLW to the development of CPP through the modulation of pulsatile GnRH release, sex-steroid synthesis, and receptor-mediated signal transduction, in interaction with neurotransmitter, energy-metabolic, and other endocrine signals.

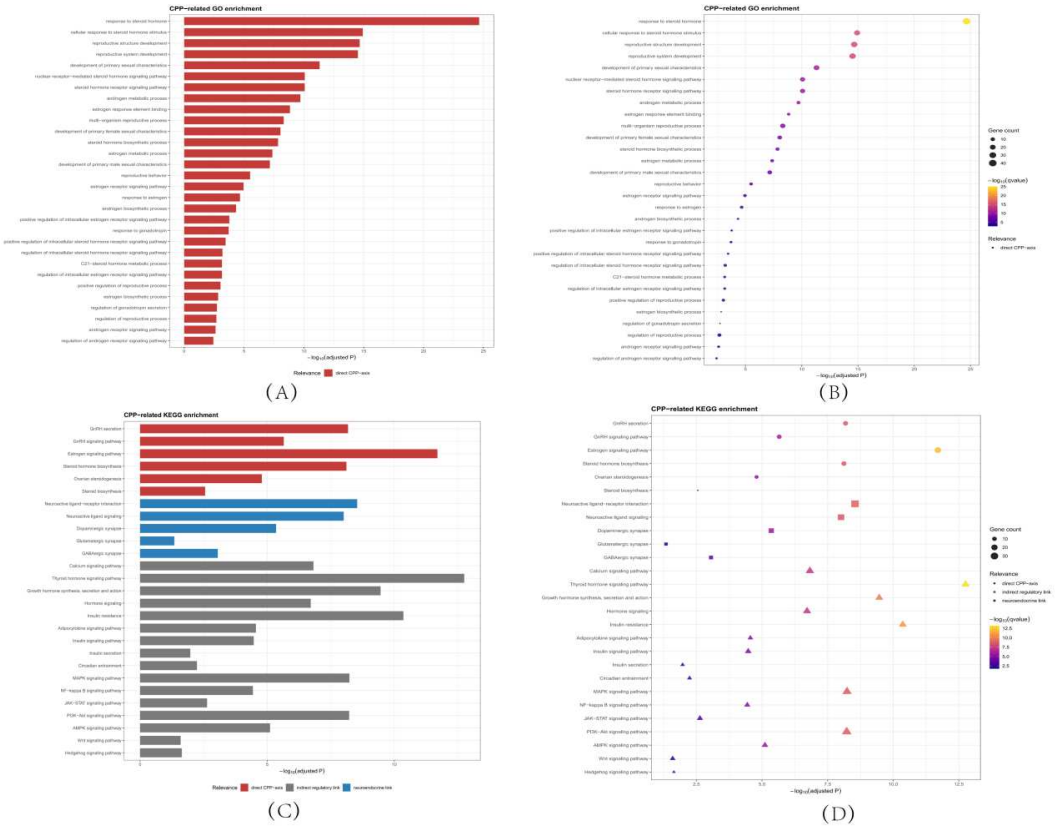

Fig. 5. CPP-relevant GO terms and KEGG pathways enriched among the potential targets of Xiaoluo Wan. KEGG pathway annotations were obtained from the KEGG database [36–38] (www.kegg.jp/kegg/kegg1.html).

3.4. "Herb–Compound–Target" Regulatory Network Analysis

The XLW "herb–compound–target" regulatory network contained 16 small-molecule nodes and 260 candidate gene nodes, connected by 658 compound–target relationships (Fig. 6). Ranked by node degree, the most highly connected candidate compounds included beta-sitosterol, sugiol, Zhebeiresinol, pelargonidin, MOL004446,

sitosterol, and harpagoside_qt; among them, beta-sitosterol showed the highest number of compound–target associations, with a degree value of 70.

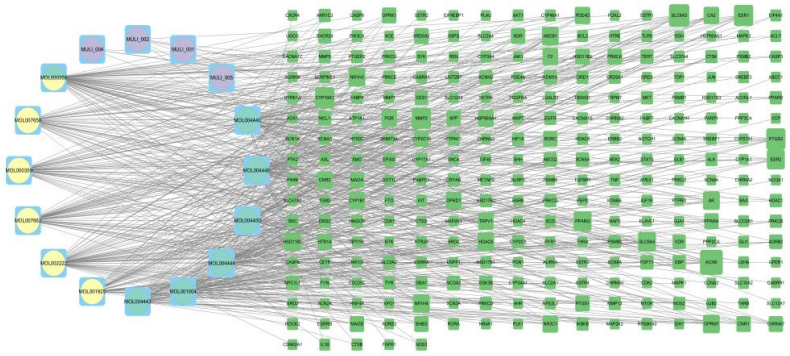

Fig. 6. "Main active compounds–core targets–major pathways" network of Xiaoluo Wan.

3.5. Molecular Docking

Seven representative small molecules and seven core proteins were selected for molecular docking, yielding 49 ligand–receptor combinations (Fig. 7; Table 2). The predicted binding affinity of beta-sitosterol to AKT1 was −10.980 kcal/mol; the affinities of sugiol to AKT1, sitosterol to SRC, and sugiol to ESR1 were −9.975, −8.715, and −8.587 kcal/mol, respectively. Representative complex structures and binding pockets—including beta-sitosterol–AKT1, beta-sitosterol–EGFR, sitosterol–SRC, and sugiol–ESR1—all exhibited binding energies below −8 kcal/mol (Fig. 8), indicating favourable predicted binding activity between the main active compounds of the formula and the core targets.

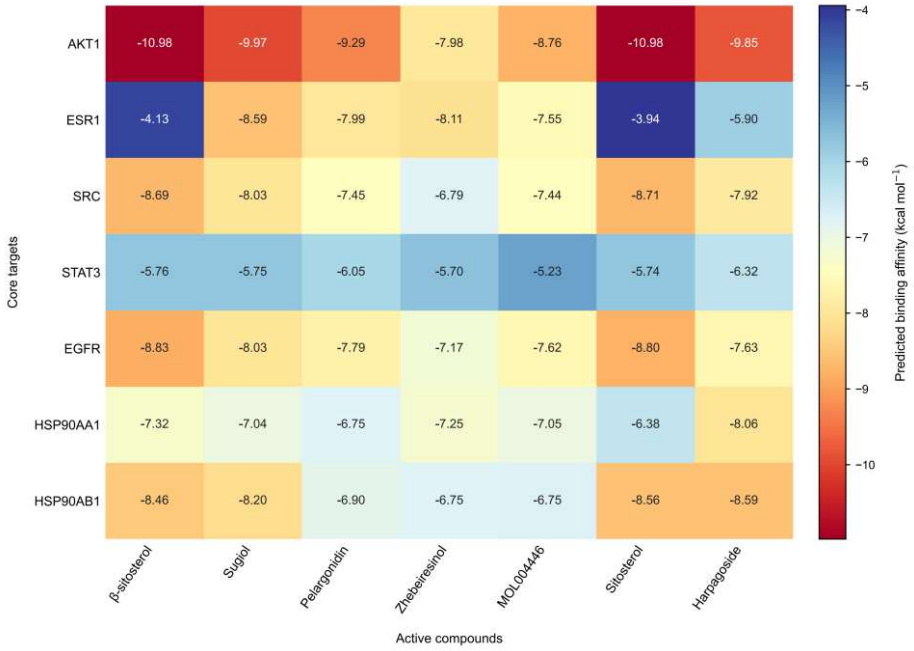

Fig. 7. Heatmap of predicted binding affinities (kcal/mol) between the active compounds of Xiaoluo Wan and the core targets.

Table 2. Representative molecular docking results.

Compound	**Core target**	**Binding affinity (kcal/mol)**
beta-Sitosterol	AKT1	−10.980
Sugiol	AKT1	−9.975
Sitosterol	SRC	−8.715
Sugiol	ESR1	−8.587
beta-Sitosterol	EGFR	< −8.0 (see Fig. 7)

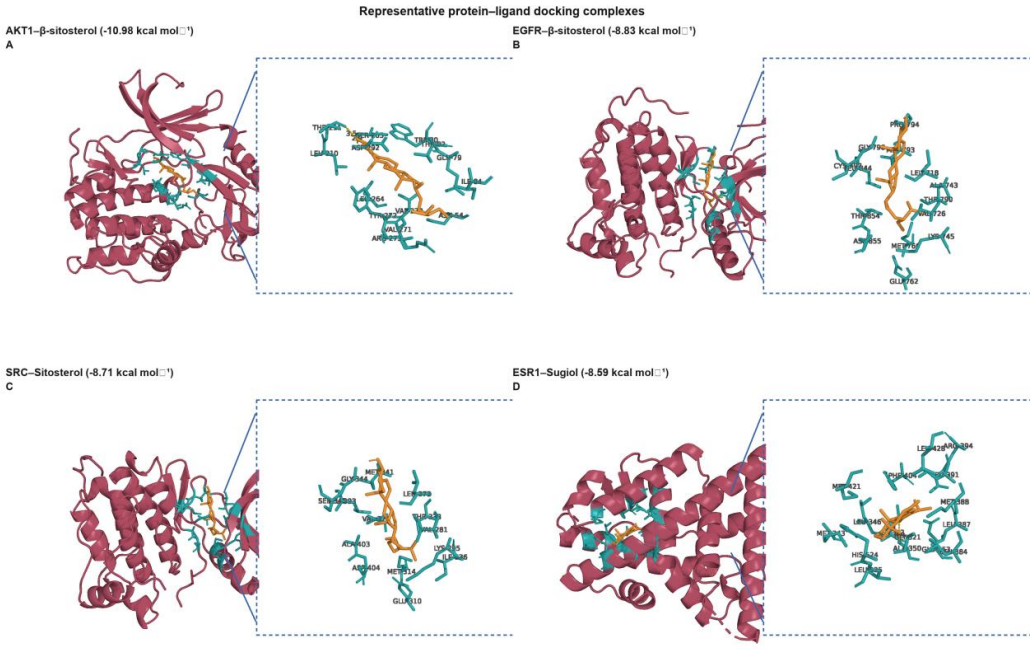

Fig. 8. Representative molecular docking models of the main active compounds of Xiaoluo Wan bound to core targets.

3.6. Safety Concentration of XLW in GT1-7 Cells

The cytotoxicity of the XLW water extract in GT1-7 cells was evaluated with the Alamar Blue assay. After 24 h of treatment, cell viability remained above 100% of the untreated control at XLW concentrations of 500–10,000 μg/mL (115.9%, 113.6%, 117.9%, and 108.4% at 500, 1,000, 5,000, and 10,000 μg/mL, respectively; all not significant vs. control), whereas viability declined to 85.4% at 12,500 μg/mL ($p < 0.05$) and to 32.4% at 15,000 μg/mL ($p < 0.0001$) (Fig. 9). Accordingly, XLW concentrations well below the cytotoxic threshold (100–500 μg/mL; 250 μg/mL for mechanistic experiments) were selected for subsequent experiments.

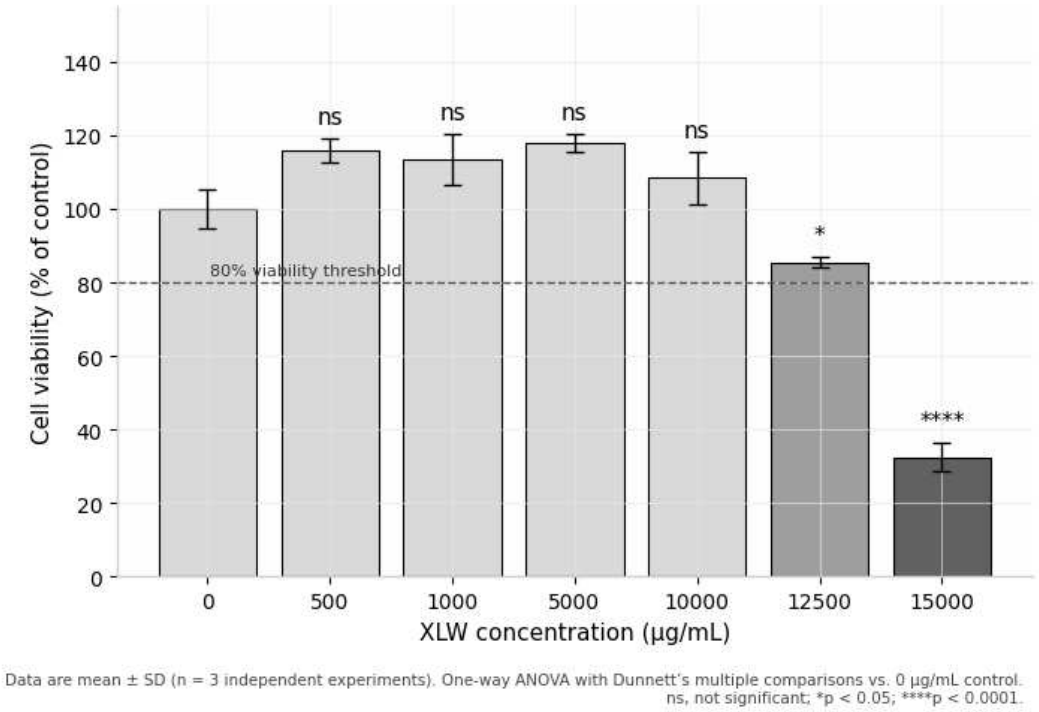

Fig. 9. Effects of the Xiaoluo Wan (XLW) water extract on the viability of GT1-7 cells (Alamar Blue assay, 24 h). Data are mean ± SD (n = 3 independent experiments); one-way ANOVA with Dunnett's multiple comparisons vs. the 0 µg/mL control. ns, not significant; *p < 0.05; ****p < 0.0001.

3.7. XLW Suppresses MCA-Induced GnRH Hypersecretion in GT1-7 Cells

Stimulation of GT1-7 cells with MCA (100 nM, 24 h) markedly increased GnRH secretion into the culture supernatant, from 6.143 ± 0.201 pg/mL in the control group to 21.470 ± 1.219 pg/mL ($p < 0.0001$), confirming successful establishment of the GnRH hypersecretion model (Fig. 10). XLW alone (250 µg/mL) did not significantly affect basal GnRH secretion (6.003 ± 0.138 pg/mL). In contrast, co-treatment with XLW almost completely abolished MCA-induced GnRH hypersecretion (5.179 ± 0.312 pg/mL; $p < 0.0001$ vs. the MCA group; one-way ANOVA, $F(3,8) = 377.6$, $p < 0.0001$).

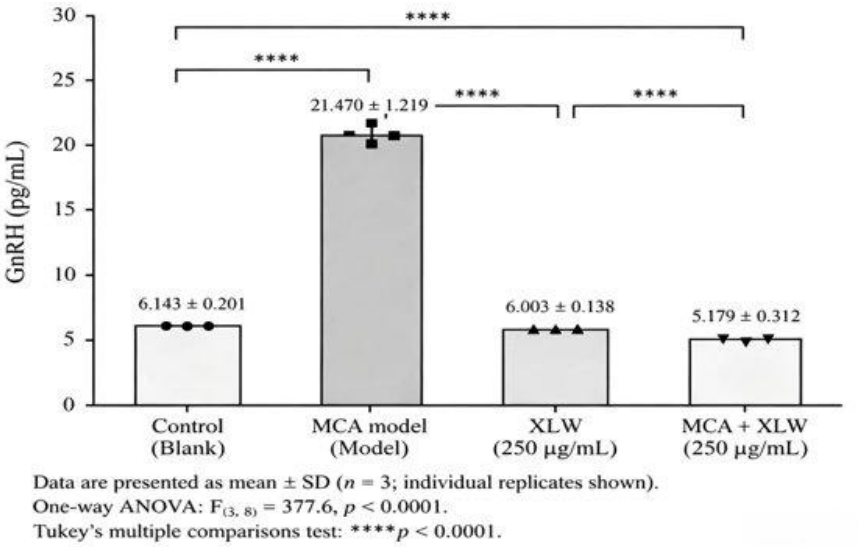

Fig. 10. Effects of XLW on MCA-induced GnRH secretion in GT1-7 cells (ELISA). Cells were treated with MCA (100 nM) in the presence or absence of XLW (250 μg/mL) for 24 h. Data are mean ± SD (n = 3; individual replicates shown); one-way ANOVA (F(3,8) = 377.6, p < 0.0001) followed by Tukey's multiple comparisons test. ****p < 0.0001.

3.8. XLW Dose-Dependently Attenuates MCA-Induced PI3K Upregulation

In dose-finding experiments, MCA stimulation increased PI3K protein expression in GT1-7 cells relative to the control (Fig. 11A). Co-treatment with XLW reduced PI3K expression in a concentration-dependent manner: densitometric quantification of the representative blot, normalised to GAPDH and expressed relative to the control, yielded relative PI3K levels of 1.68 in the MCA group and 1.01, 0.78, and 0.76 in the MCA + XLW 100, 250, and 500 μg/mL groups, respectively (Fig. 11B). The 250 μg/mL concentration was therefore carried forward as the interventional dose for subsequent mechanistic experiments, consistent with the GnRH secretion assays.

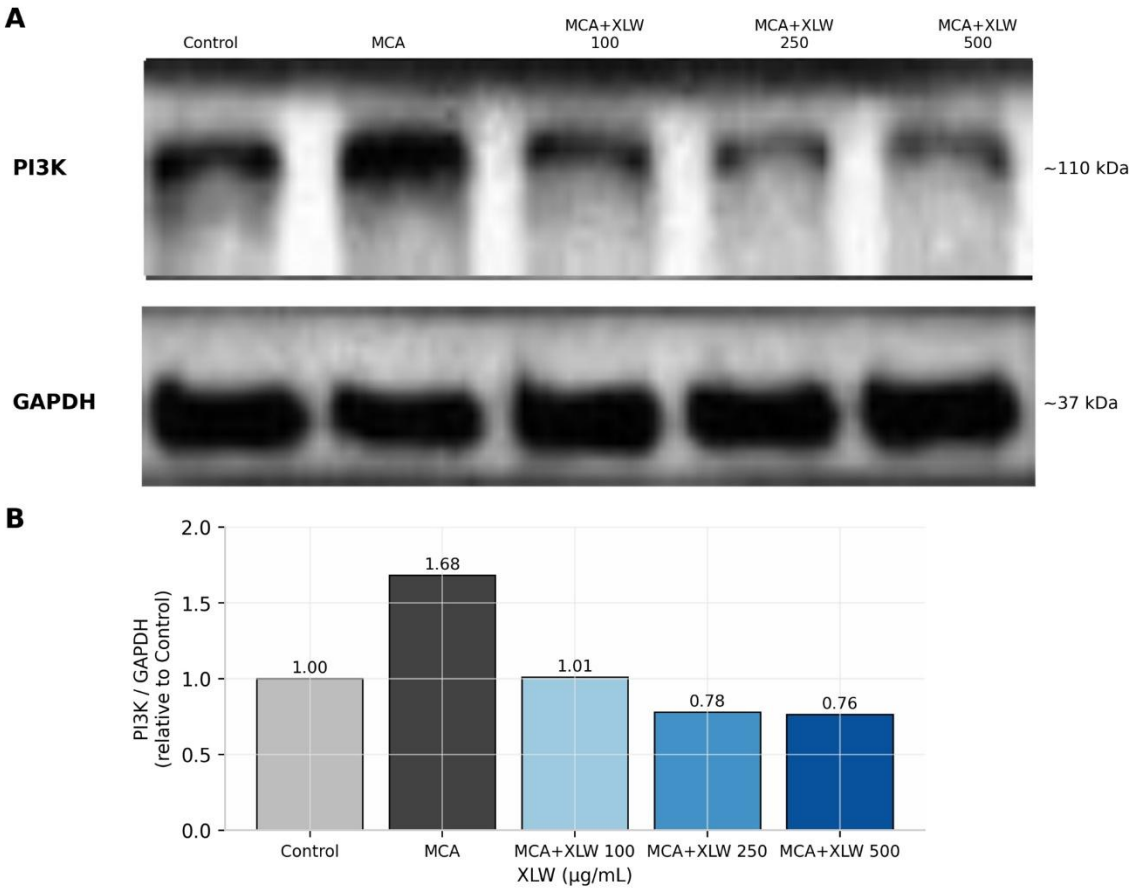

Fig. 11. Dose-dependent effect of XLW on MCA-induced PI3K expression in GT1-7 cells. (A) Representative Western blots of PI3K and GAPDH in the control, MCA model, and MCA + XLW (100, 250, and 500 μg/mL) groups. (B) Densitometric quantification of the blot shown in (A); PI3K band intensities were normalised to GAPDH and expressed relative to the control group.

3.9. XLW Modulates the TGR5–PI3K/Akt Signalling Pathway: Involvement of TGR5

Western blot analyses of the four-group mechanistic experiment showed that MCA stimulation increased TGR5 and PI3K protein expression and enhanced Akt phosphorylation (Ser473) in GT1-7 cells, consistent with activation of the TGR5–PI3K/Akt cascade (Fig. 12). XLW treatment (250 μg/mL) attenuated the MCA-induced changes in PI3K expression and Akt phosphorylation, whereas XLW alone had no marked effect on these indices in unstimulated cells. GPER, a membrane oestrogen receptor previously implicated in the regulation of GnRH secretion, was also examined

and showed a tendency toward reduced expression after MCA stimulation that was restored by XLW co-treatment.

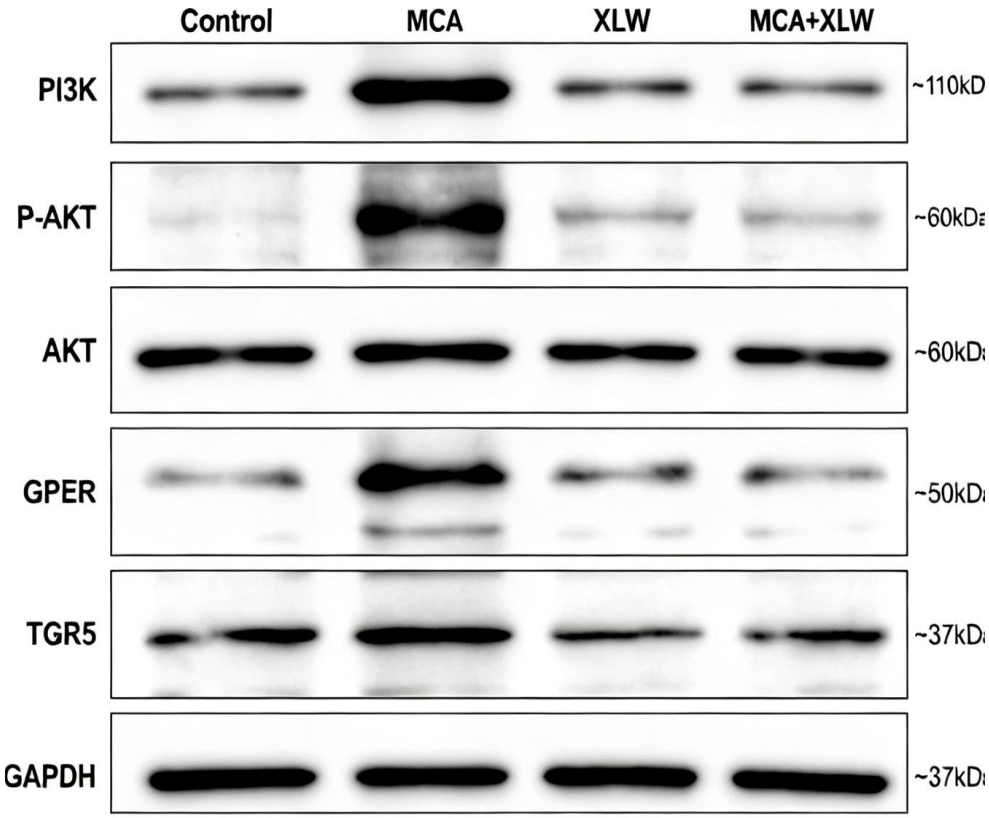

Fig. 12. Representative Western blots of PI3K, phospho-Akt (Ser473), total Akt, GPER, TGR5, and GAPDH in GT1-7 cells of the control, MCA model, XLW alone (250 μg/mL), and MCA + XLW (250 μg/mL) groups.

To interrogate the contribution of TGR5, the TGR5-specific antagonist SBI-115 (10 μM) was applied in the presence of MCA (Fig. 13). Under TGR5 blockade, PI3K expression and Akt phosphorylation in MCA-stimulated cells were reduced, and the additional modulatory effect of XLW on PI3K expression and Akt phosphorylation was attenuated compared with MCA + XLW without SBI-115, indicating that the action of XLW on this pathway is at least partly dependent on TGR5 signalling. TGR5 protein abundance was likewise lowest in the MCA + XLW group and was partially restored when TGR5 was pharmacologically blocked, a pattern consistent with reduced receptor engagement under combined treatment.

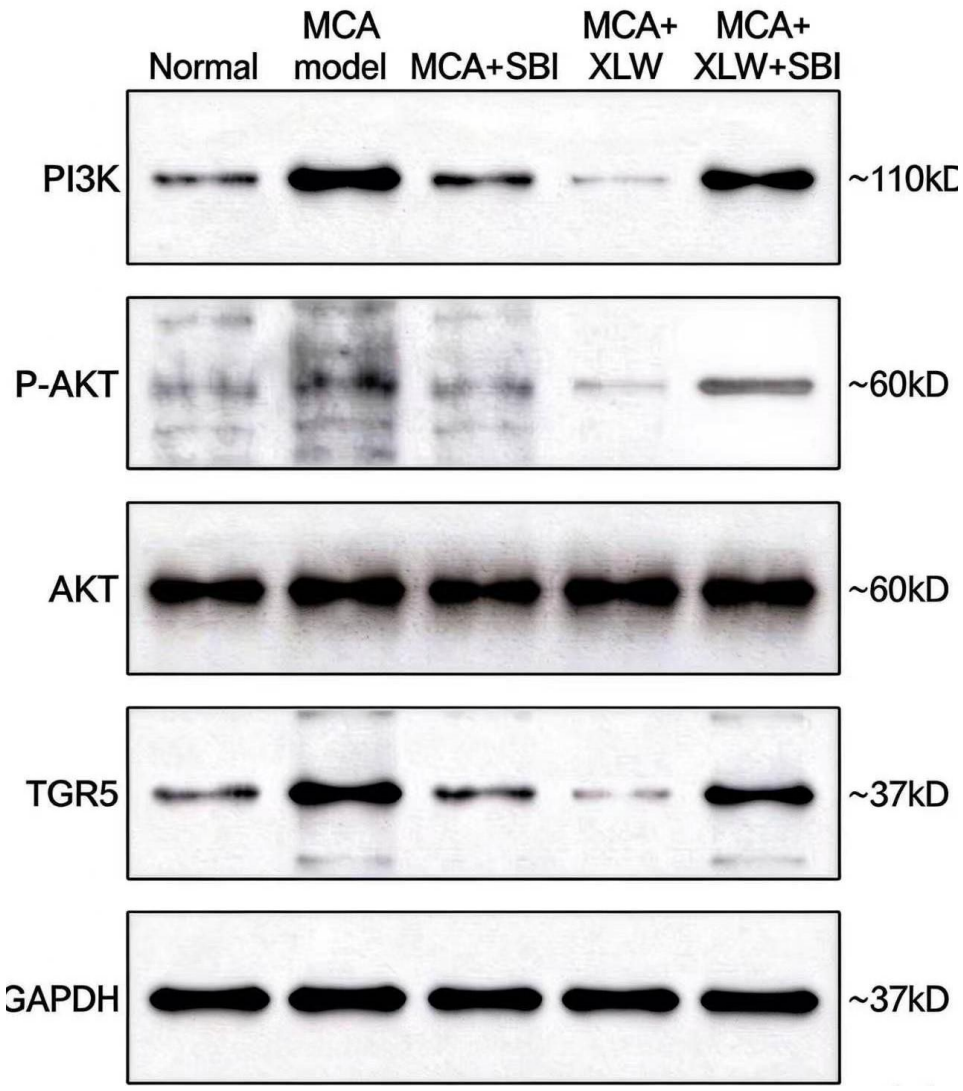

Fig. 13. Representative Western blots of PI3K, phospho-Akt (Ser473), total Akt, TGR5, and GAPDH in GT1-7 cells of the normal control, MCA model, MCA + SBI-115 (10 μM), MCA + XLW (250 μg/mL), and MCA + XLW + SBI-115 groups.

4. Discussion

In this study, we integrated network pharmacology, molecular docking, and in vitro experiments to characterise the potential pharmacological mechanism of XLW, a classical TCM formula clinically used for CPP. Sixteen candidate compounds were linked to 260 CPP-related targets, and topological analysis identified a core target module—SRC, ESR1, AKT1, STAT3, and EGFR—that is highly enriched in GnRH,

oestrogen, and PI3K/Akt-related signalling. Molecular docking supported strong direct interactions between the most highly connected compounds and these core targets. Critically, in MCA-stimulated GT1-7 hypothalamic GnRH neuronal cells, XLW abolished bile acid-induced GnRH hypersecretion and attenuated TGR5–PI3K/Akt activation, an effect that was weakened by the TGR5 antagonist SBI-115. Taken together, the data delineate a coherent "multi-compound–multi-target–multi-pathway" profile through which XLW may restrain premature HPGA activation, and provide initial experimental support for its intersection with the bile acid–TGR5–PI3K/Akt axis.

4.1. Core Targets Converge on GnRH- and PI3K/Akt-Centred Neuroendocrine Regulation

The five highest-centrality core targets are biologically plausible effectors in CPP. AKT1 and PIK3CA constitute the central nodes of the PI3K/Akt pathway, which governs the excitability, gene expression, and secretory activity of hypothalamic neurons, including kisspeptin and GnRH neurons [15,16]. SRC family kinases participate in growth-factor and G-protein-coupled receptor signalling upstream of PI3K/Akt and MAPK cascades; the concurrent enrichment of MAPK1 and MAPK3 in the core target set reinforces this interpretation. ESR1 mediates oestrogen feedback on the HPGA, and dysregulated oestrogen signalling is intimately linked to pubertal timing, whereas STAT3 is a well-established downstream effector of leptin-receptor signalling in hypothalamic neurons and thereby couples nutritional status to reproductive function. EGFR and ERBB2, together with the enriched "EGFR tyrosine kinase inhibitor resistance" and "HIF-1" pathways, point to growth-factor and energy-sensing crosstalk. The enrichment of GnRH secretion and GnRH signalling pathways, oestrogen signalling, steroid hormone biosynthesis, and ovarian steroidogenesis directly mirrors the terminal effector programme of the HPGA, while the enrichment of dopaminergic, GABAergic, glutamatergic, and calcium signalling pathways is consistent with the synaptic and neurotransmitter control of the GnRH pulse generator. Importantly, the significant enrichment of insulin signalling, insulin resistance, and adipocytokine signalling supports a mechanistic bridge between the metabolic disturbance of obesity and premature pubertal activation—precisely the clinical context in which XLW is most often applied.

4.2. Key Compounds and Their Putative Actions

Beta-sitosterol was the most highly connected compound in the network (degree = 70) and showed the strongest predicted affinity for AKT1 (−10.980 kcal/mol). As a phytosterol shared by several component herbs, beta-sitosterol has documented phytoestrogenic, anti-inflammatory, and lipid-modulating properties, all of which are relevant to the metabolic–reproductive interface of CPP. Sitosterol and sugiol likewise showed strong affinities for SRC and ESR1/AKT1, respectively, suggesting that sterol- and diterpene-type constituents jointly tune the core signalling module. Harpagoside, a characteristic iridoid glycoside of Scrophulariae Radix, contributes anti-inflammatory and neuroendocrine-modulating activities attributed to the monarch herb of the formula [19]. Zhebeiresinol and alkaloid constituents of Fritillariae Thunbergii Bulbus (e.g., peimine and peiminine) have been reported to regulate lipid metabolism and PI3K/Akt/mTOR signalling, providing a plausible chemical basis for the "phlegm-resolving" function of the minister herb [20,21]. Although Ostreae Concha is a shell-derived medicinal dominated by inorganic salts, its network-retrieved constituents, together with its recognised content of taurine and trace elements such as zinc and selenium, may support hypothalamic neuronal homeostasis and gonadal development [18].

4.3. Experimental Support for Intersection with the Bile Acid–MCA–TGR5–PI3K/Akt Axis

The most notable context for our findings is the recently established role of bile acid signalling in pubertal timing. TGR5 is expressed in hypothalamic kisspeptin neurons, its activation stimulates GnRH release ex vivo, and its early overexpression in the arcuate nucleus advances puberty in female rats [13]. Wang et al. further demonstrated that MCA species—bile acids that accumulate in the hypothalamus under high-fat-diet conditions—activate TGR5 on GnRH neurons and enhance GnRH expression through the TGR5–PI3K/Akt–mTOR cascade, and that lowering MCA delays, whereas elevating MCA accelerates, pubertal onset in female mice [14]. Our in vitro data are directly consistent with this framework: MCA robustly stimulated GnRH secretion from GT1-7 cells, and

XLW—whose network-predicted core targets centre on the PI3K/Akt module and whose constituents bind AKT1 with high predicted affinity—suppressed this hypersecretion while attenuating TGR5–PI3K/Akt activation in a concentration-dependent manner. The observation that the TGR5 antagonist SBI-115 weakened the effect of XLW on PI3K/Akt signalling further supports the participation of TGR5 in the action of the formula, although it should be noted that if MCA signalling is already blocked at the receptor level, a reduced incremental effect of XLW would also be expected; TGR5 knockdown approaches will be required to more stringently establish target dependence.

From the perspective of TCM theory, this mechanism also provides a modern molecular correlate for the classical indication of XLW. The "yin deficiency with phlegm coagulation" pattern corresponds closely to the pathophysiology of obesity-related CPP, in which aberrant MCA accumulation and TGR5 overactivation may be viewed as molecular correlates of "phlegm turbidity clouding the clear orifices" and "effulgent yin-deficiency fire", respectively [17,18]. Whether XLW also acts upstream by reshaping bile acid metabolism—for example, by reducing circulating and hypothalamic MCA levels—remains to be tested in high-fat-diet-induced animal models with targeted bile acid metabolomics, which constitutes the next step of our research programme.

4.4. Limitations

Several limitations should be acknowledged. First, network pharmacology is inherently predictive: compound and target collections depend on the coverage and update status of public databases, and animal/mineral-derived medicinals such as Ostreae Concha remain under-represented in these resources, so the retrieved six compounds may not fully capture its material basis (e.g., bioactive peptides and taurine). Second, target prediction tools such as SwissTargetPrediction provide probabilistic associations that require experimental confirmation. Third, molecular docking affinities indicate potential binding but do not demonstrate functional engagement in a cellular or organismal context. Fourth, the in vitro validation reported here is preliminary: it was conducted at a single MCA concentration over a 24-h window, the chemical composition of the water extract batch was not standardised against quantified marker compounds, and comprehensive densitometric quantification of Western blot endpoints across

independent biological replicates, RT-qPCR analyses of GnRH/Kiss1/KISS1R/TGR5, and TGR5 gene-silencing experiments are still in progress. Finally, cell-based findings in GT1-7 neurons cannot be directly extrapolated to the in vivo regulation of pubertal timing; animal studies with targeted bile acid metabolomics and hypothalamic transcriptomics are warranted.

5. Conclusions

This study suggests that Xiaoluo Wan counteracts central precocious puberty through a multi-component, multi-target, and multi-pathway mechanism centred on the SRC–ESR1–AKT1–STAT3–EGFR core module and converging on PI3K/Akt, GnRH, oestrogen, and metabolic signalling pathways. Beta-sitosterol, sugiol, sitosterol, and harpagoside emerged as priority compounds with strong predicted binding to core targets. In vitro experiments in MCA-stimulated GT1-7 GnRH neuronal cells support the conclusion that XLW suppresses bile acid-driven GnRH hypersecretion and attenuates TGR5–PI3K/Akt signalling, positioning the formula as a rational candidate for intersecting the MCA–TGR5–PI3K/Akt axis that links obesity to premature pubertal activation. These findings provide a mechanistic framework and a prioritised set of compounds and targets for further in-depth in vitro and in vivo validation.

Declarations

Ethics approval and consent to participate: Not applicable. The network pharmacology analyses were based exclusively on publicly available databases, and the in vitro experiments used an established immortalised cell line; no human participants, human data, or animals were involved.

Consent for publication: Not applicable.

Availability of data and materials: All data generated or analysed during this study are included in this published article and its figures. The raw target and enrichment lists are available from the corresponding author on reasonable request.

Competing interests: The authors declare that they have no competing interests.

Funding: This work was supported by the "Jiebang Guashuai" (Open Competition Mechanism) Graduate Innovation Capacity Enhancement Programme of Guangzhou University of Chinese Medicine [grant number to be assigned] and the 2025 Clinical–Basic Science and Technology Innovation Project of Guangdong Medical University (grant No. A012500054).

Authors' contributions: JK performed the network pharmacology analysis, molecular docking, and cell experiments, and drafted the manuscript. ZW contributed to bioinformatics analysis and study design. Jianlei Liu, Chunmei He, and Shanshan He contributed to the cell experiments and data curation. SW authenticated the crude drugs. HL contributed to data curation and statistical organisation. Jun Lu co-supervised the study and acquired funding. SM conceived and supervised the study, interpreted the results from the perspective of clinical TCM, and critically revised the manuscript. All authors read and approved the final manuscript.

Acknowledgements: The authors thank the Precision Oncology Key Laboratory, the Institute of Translational Medicine, and the Cellular Immunology Experimental Center of Foshan Fosun Chancheng Hospital for technical support.

References

[1] Kaplowitz P, Bloch C; Section on Endocrinology, American Academy of Pediatrics. Evaluation and referral of children with signs of early puberty. Pediatrics. 2016;137(1):e20153732.

[2] Latronico AC, Brito VN, Carel JC. Causes, diagnosis, and treatment of central precocious puberty. Lancet Diabetes Endocrinol. 2016;4(3):265–274.

[3] Brix N, Ernst A, Lauridsen LLB, Parner ET, Arah OA, Olsen J, et al. Timing of puberty in boys and girls: a population-based study. Paediatr Perinat Epidemiol. 2019;33(1):70–78.

[4] Li W, Liu Q, Deng X, Chen Y, Liu W, Story M. Association between obesity and precocious puberty: a systematic review and meta-analysis. Int J Environ Res Public Health. 2017;14(10):1266.

[5] Reinehr T, Roth CL. Is there a causal relationship between obesity and puberty? Lancet Child Adolesc Health. 2019;3(1):44–54.

[6] Frisch RE, McArthur JW. Menstrual cycles: fatness as a determinant of minimum weight for height necessary for their maintenance or onset. Science. 1974;185(4155):949–951.

[7] Seminara SB, Messager S, Chatzidaki EE, Thresher RR, Acierno JS Jr, Shagoury JK, et al. The GPR54 gene as a regulator of puberty. N Engl J Med. 2003;349(17):1614–1627.

[8] Abreu AP, Dauber A, Macedo DB, Noel SD, Brito VN, Gill JC, et al. Central precocious puberty caused by mutations in the imprinted gene MKRN3. N Engl J Med. 2013;368(26):2467–2475.

[9] Kawamata Y, Fujii R, Hosoya M, Harada M, Yoshida H, Miwa M, et al. A G protein-coupled receptor responsive to bile acids. J Biol Chem. 2003;278(11):9435–9440.

[10] Thomas C, Gioiello A, Noriega L, Strehle L, Oury J, Rizzo G, et al. TGR5-mediated bile acid sensing controls glucose homeostasis. Cell Metab. 2009;10(3):167–177.

[11] Watanabe M, Houten SM, Mataki C, Christoffolete MA, Kim BW, Sato H, et al. Bile acids induce energy expenditure by promoting intracellular thyroid hormone activation. Nature. 2006;439(7075):484–489.

[12] Keitel V, Häussinger D. Perspective: TGR5 (Gpbar-1) in liver physiology and disease. Clin Res Hepatol Gastroenterol. 2012;36(5):412–419.

[13] Vanden Brink H, Vandeputte D, Brito IL, Ronnekleiv OK, Roberson MS, Lomniczi A. Changes in the bile acid pool and timing of female puberty: potential novel role of hypothalamic TGR5. Endocrinology. 2024;165(9):bqae098.

[14] Wang S, Huang K, Liu A, Wang S, Jiang R, Chen W, et al. Muricholic acid mediates puberty initiation via the hypothalamic TGR5 signaling pathway. Proc Natl Acad Sci U S A. 2025;122(37):e2511404122.

[15] Manning BD, Toker A. AKT/PKB signaling: navigating the network. Cell. 2017;169(3):381–405.

[16] Manning BD, Cantley LC. AKT/PKB signaling: navigating downstream. Cell. 2007;129(7):1261–1274.

[17] Cheng ZL. Yi Xue Xin Wu (Medical Insights). Qing Dynasty, 1732 (classical Chinese medical text).

[18] National Pharmacopoeia Commission. Pharmacopoeia of the People's Republic of China (2020 Edition), Volume I. Beijing: China Medical Science Press; 2020.

[19] Li YM, Han ZH, Jiang SH, Jiang Y, Yao SD, Zhu DY. Fast repairing of oxidative DNA damage by phenylpropanoid glycosides from Scrophularia ningpoensis. Chin Chem Lett. 2000;11(7):613–616.

[20] Hao DC, Gu XJ, Xiao PG, Peng Y. Phytochemical and biological research of Fritillaria medicinal resources. Chin J Nat Med. 2013;11(4):330–344.

[21] Zhang LW, Su YF, Wu CF, Wu YH, Gong ZH. Inhibitory effects of total and alkaloidal fractions of the cultivated Bulbus Fritillariae ussuriensis on dopamine D2 receptor. J Ethnopharmacol. 2010;127(2):264–271.

[22] Hopkins AL. Network pharmacology: the next paradigm in drug discovery. Nat Chem Biol. 2008;4(11):682–690.

[23] Ru J, Li P, Wang J, Zhou W, Li B, Huang C, et al. TCMSP: a database of systems pharmacology for drug discovery from herbal medicines. J Cheminform. 2014;6:13.

[24] Liu Z, Guo F, Wang Y, Li C, Zhang X, Li H, et al. BATMAN-TCM: a bioinformatics analysis tool for molecular mechanism of traditional Chinese medicine. Sci Rep. 2016;6:21146.

[25] Daina A, Michielin O, Zoete V. SwissADME: a free web tool to evaluate pharmacokinetics, drug-likeness and medicinal chemistry friendliness of small molecules. Sci Rep. 2017;7:42717.

[26] Daina A, Michielin O, Zoete V. SwissTargetPrediction: updated data and new features for efficient prediction of protein targets of small molecules. Nucleic Acids Res. 2019;47(W1):W357–W364.

[27] The UniProt Consortium. UniProt: the universal protein knowledgebase in 2021. Nucleic Acids Res. 2021;49(D1):D480–D489.

[28] Stelzer G, Rosen N, Plaschkes I, Zimmerman S, Twik M, Fishilevich S, et al. The GeneCards suite: from gene data mining to disease genome sequence analyses. Curr Protoc Bioinformatics. 2016;54:1.30.1–1.30.33.

[29] Wishart DS, Feunang YD, Guo AC, Lo EJ, Marcu A, Grant JR, et al. DrugBank 5.0: a major update to the DrugBank database for 2018. Nucleic Acids Res. 2018;46(D1):D1074–D1082.

[30] Piñero J, Bravo À, Queralt-Rosinach N, Gutiérrez-Sacristán A, Deu-Pons J, Centeno E, et al. DisGeNET: a comprehensive platform integrating information on human disease-associated genes and variants. Nucleic Acids Res. 2017;45(D1):D833–D839.

[31] Amberger JS, Bocchini CA, Scott AF, Hamosh A. OMIM.org: leveraging knowledge across phenotype–gene relationships. Nucleic Acids Res. 2019;47(D1):D1038–D1043.

[32] Shannon P, Markiel A, Ozier O, Baliga NS, Wang JT, Ramage D, et al. Cytoscape: a software environment for integrated models of biomolecular interaction networks. Genome Res. 2003;13(11):2498–2504.

[33] Szklarczyk D, Kirsch R, Koutrouli M, Nastou KC, Mehryary F, Hachilif R, et al. The STRING database in 2023: protein–protein association networks and functional enrichment analyses for any sequenced genome of interest. Nucleic Acids Res. 2023;51(D1):D638–D646.

[34] Tang Y, Li M, Wang J, Pan Y, Wu FX. CytoNCA: a cytoscape plugin for centrality analysis and evaluation of protein interaction networks. Biosystems. 2015;127:67–72.

[35] Sherman BT, Hao M, Qiu J, Jiao X, Baseler MW, Lane HC, et al. DAVID: a web server for functional enrichment analysis and functional annotation of gene lists (2021 update). Nucleic Acids Res. 2022;50(W1):W216–W221.

[36] Kanehisa M, Goto S. KEGG: Kyoto encyclopedia of genes and genomes. Nucleic Acids Res. 2000;28(1):27–30.

[37] Kanehisa M. Toward understanding the origin and evolution of cellular organisms. Protein Sci. 2019;28(11):1947–1951.

[38] Kanehisa M, Furumichi M, Sato Y, Kawashima M, Ishiguro-Watanabe M. KEGG for taxonomy-based analysis of pathways and genomes. Nucleic Acids Res. 2023;51(D1):D587–D592.

[39] Ashburner M, Ball CA, Blake JA, Botstein D, Butler H, Cherry JM, et al. Gene ontology: tool for the unification of biology. The Gene Ontology Consortium. Nat Genet. 2000;25(1):25–29.

[40] Kim S, Chen J, Cheng T, Gindulyte A, He J, He S, et al. PubChem 2023 update. Nucleic Acids Res. 2023;51(D1):D1373–D1380.

[41] Burley SK, Bhikadiya C, Bi C, Bittrich S, Chen L, Crichlow GV, et al. RCSB Protein Data Bank: powerful new tools for exploring 3D structures of biological macromolecules for basic and applied research and education. Nucleic Acids Res. 2021;49(D1):D437–D451.

[42] Trott O, Olson AJ. AutoDock Vina: improving the speed and accuracy of docking with a new scoring function, efficient optimization, and multithreading. J Comput Chem. 2010;31(2):455–461.

[43] Eberhardt J, Santos-Martins D, Tillack AF, Forli S. AutoDock Vina 1.2.0: new docking methods, expanded force field, and Python bindings. J Chem Inf Model. 2021;61(8):3891–3898.

[44] The PyMOL Molecular Graphics System, Version 3.1. Schrödinger, LLC.

[45] Mellon PL, Windle JJ, Goldsmith PC, Padula CA, Roberts JL, Weiner RI. Immortalization of hypothalamic GnRH neurons by genetically targeted tumorigenesis. Neuron. 1990;5(1):1–10.

Supplementary Material

Supplementary Fig. S1. Base peak intensity (BPI) chromatogram of the Xiaoluo Wan water extract acquired by UHPLC-Q-Orbitrap HRMS in positive ESI mode (see file FigS1_LCMS_pos.png).

Supplementary Fig. S2. Base peak intensity (BPI) chromatogram of the Xiaoluo Wan water extract acquired by UHPLC-Q-Orbitrap HRMS in negative ESI mode (see file FigS2_LCMS_neg.png).

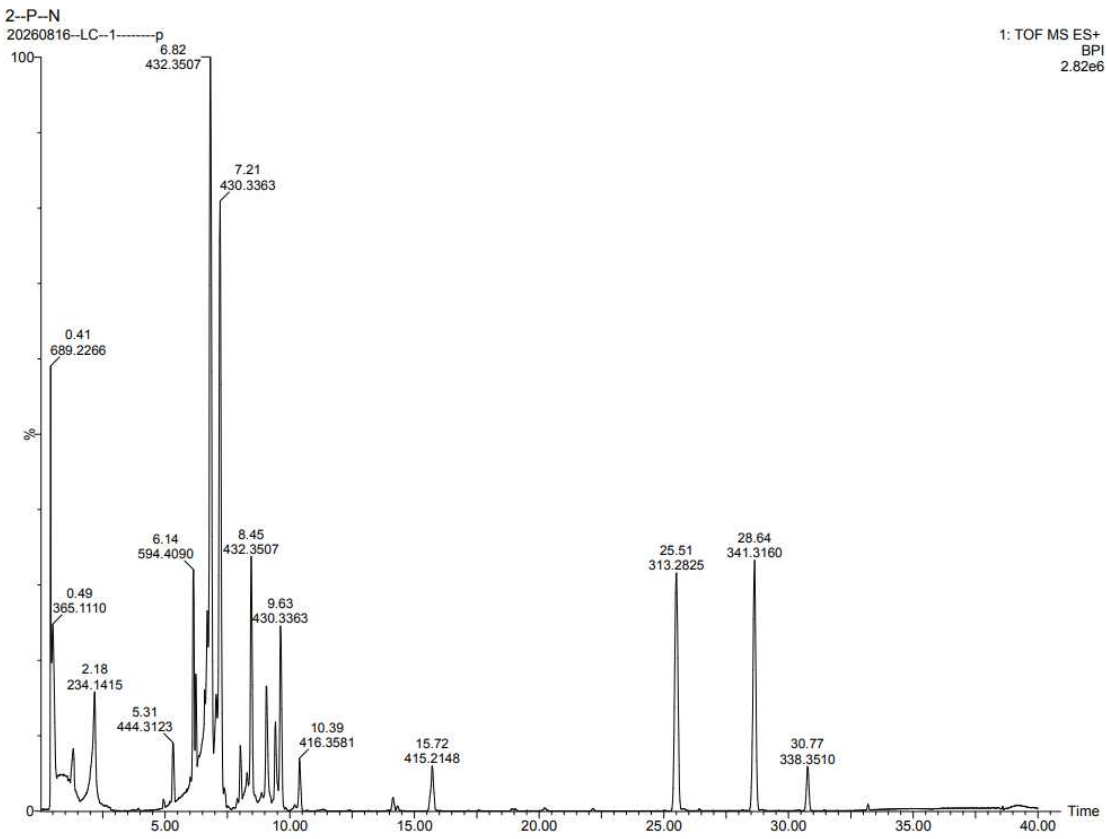
2--P--N
20260816--LC--1--------p
1: TOF MS ES+
BPI
2.82e6
100
%
0
6.82
432.3507
7.21
430.3363
0.41
689.2266
6.14
594.4090
8.45
432.3507
0.49
365.1110
9.63
430.3363
2.18
234.1415
5.31
444.3123
10.39
416.3581
15.72
415.2148
25.51
313.2825
28.64
341.3160
30.77
338.3510
5.00
10.00
15.00
20.00
25.00
30.00
35.00
40.00
Time

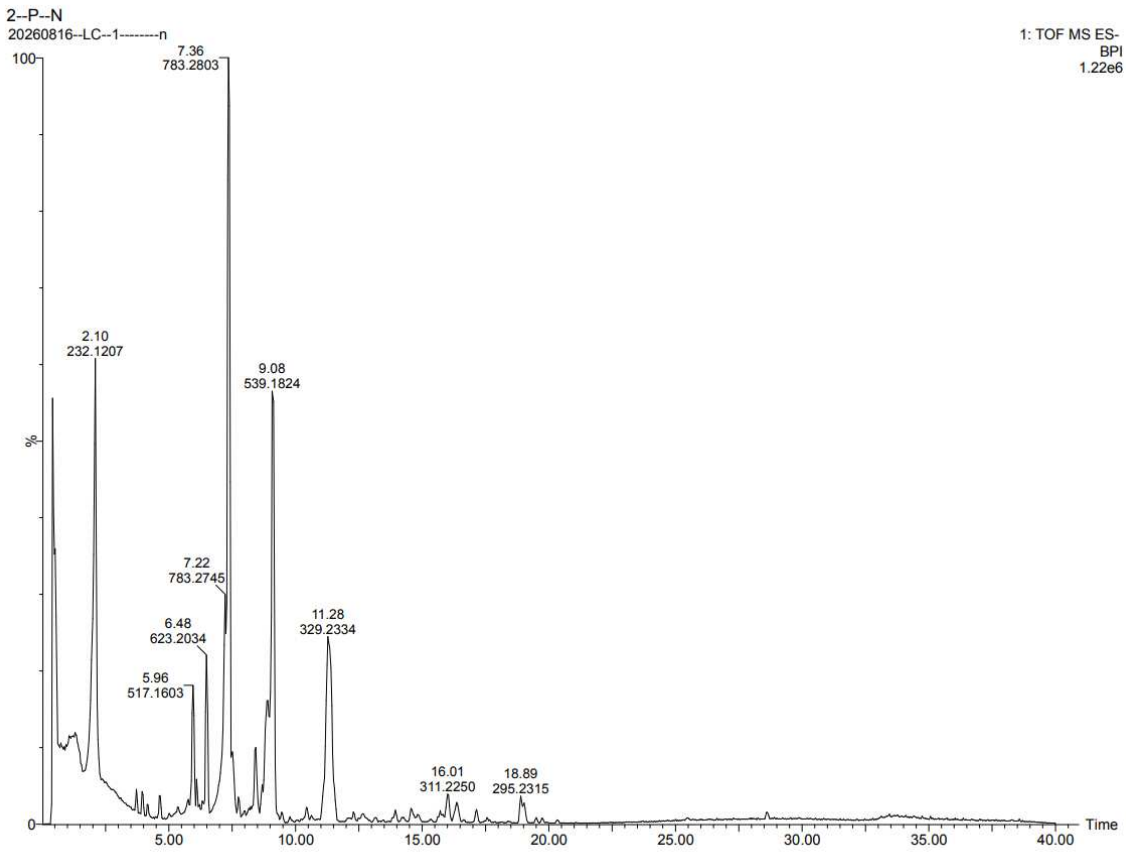
2--P--N
20260816--LC--1--------n
1: TOF MS ES-
BPI
1.22e6
100
%
0
7.36
783.2803
2.10
232.1207
9.08
539.1824
7.22
783.2745
6.48
623.2034
5.96
517.1603
11.28
329.2334
16.01
311.2250
18.89
295.2315
5.00
10.00
15.00
20.00
25.00
30.00
35.00
40.00
Time